



ORIGINAL RESEARCH

## PIP<sub>2</sub> Improves Cerebral Blood Flow in a Mouse Model of Alzheimer's Disease

Amreen Mughal <sup>1</sup>, Osama F. Harraz <sup>1,2</sup>, Albert L. Gonzales<sup>1,3</sup>,  
David Hill-Eubanks<sup>1</sup>, Mark T. Nelson<sup>1,2,4,\*</sup>

<sup>1</sup>Department of Pharmacology, Larner College of Medicine, University of Vermont, Burlington, VT, USA;

<sup>2</sup>Vermont Center for Cardiovascular and Brain Health, University of Vermont, Burlington, VT, USA;

<sup>3</sup>Department of Physiology and Cell Biology, University of Nevada, Reno, School of Medicine, Reno, NV, USA;

<sup>4</sup>Division of Cardiovascular Sciences, University of Manchester, Manchester, UK

A.M. and O.F.H. are co-first authors who contributed equally.

\*Address correspondence to M.T.N. (e-mail: mark.nelson@uvm.edu)

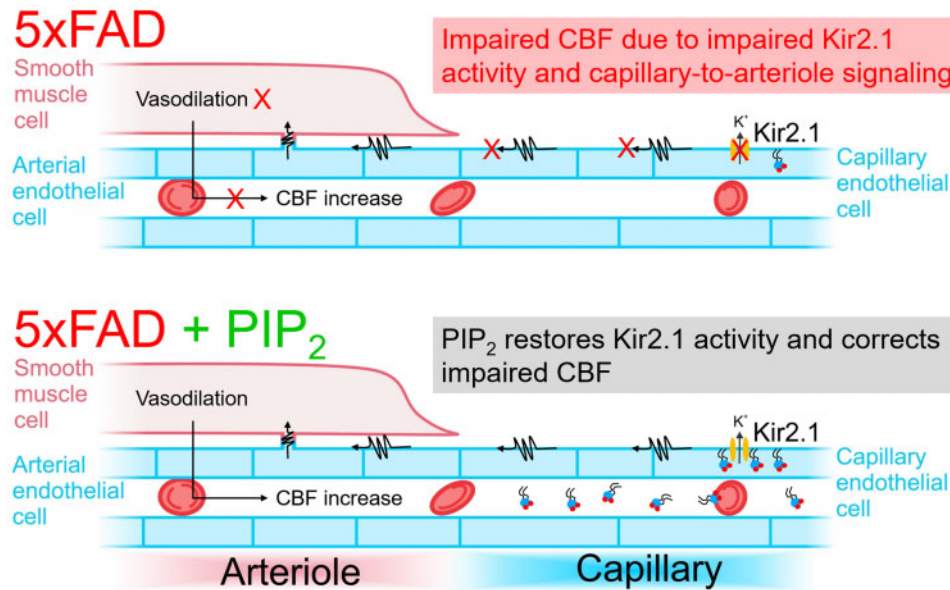
### Abstract

Alzheimer's disease (AD) is a leading cause of dementia and a substantial healthcare burden. Despite this, few treatment options are available for controlling AD symptoms. Notably, neuronal activity-dependent increases in cortical cerebral blood flow (CBF; functional hyperemia) are attenuated in AD patients, but the associated pathological mechanisms are not fully understood at the molecular level. A fundamental mechanism underlying functional hyperemia is activation of capillary endothelial inward-rectifying K<sup>+</sup> (Kir2.1) channels by neuronally derived potassium (K<sup>+</sup>), which evokes a retrograde capillary-to-arteriole electrical signal that dilates upstream arterioles, increasing blood delivery to downstream active regions. Here, using a mouse model of familial AD (5xFAD), we tested whether this impairment in functional hyperemia is attributable to reduced activity of capillary Kir2.1 channels. *In vivo* CBF measurements revealed significant reductions in whisker stimulation (WS)-induced and K<sup>+</sup>-induced hyperemic responses in 5xFAD mice compared with age-matched controls. Notably, measurements of whole-cell currents in freshly isolated 5xFAD capillary endothelial cells showed that Kir2.1 current density was profoundly reduced, suggesting a defect in Kir2.1 function. Because Kir2.1 activity absolutely depends on binding of phosphatidylinositol 4,5-bisphosphate (PIP<sub>2</sub>) to the channel, we hypothesized that capillary Kir2.1 channel impairment could be corrected by exogenously supplying PIP<sub>2</sub>. As predicted, a PIP<sub>2</sub> analog restored Kir2.1 current density to control levels. More importantly, systemic administration of PIP<sub>2</sub> restored K<sup>+</sup>-induced CBF increases and WS-induced functional hyperemic responses in 5xFAD mice. Collectively, these data provide evidence that PIP<sub>2</sub>-mediated restoration of capillary endothelial Kir2.1 function improves neurovascular coupling and CBF in the setting of AD.

Submitted: 26 January 2021; Revised: 16 February 2021; Accepted: 16 February 2021

© The Author(s) 2021. Published by Oxford University Press on behalf of American Physiological Society.

This is an Open Access article distributed under the terms of the Creative Commons Attribution Non-Commercial License (<http://creativecommons.org/licenses/by-nc/4.0/>), which permits non-commercial re-use, distribution, and reproduction in any medium, provided the original work is properly cited. For commercial re-use, please contact [journals.permissions@oup.com](mailto:journals.permissions@oup.com)



**Key words:** Alzheimer's disease; cerebral blood flow; endothelial cells; Kir2.1; PIP<sub>2</sub>; potassium channels; phosphoinositides; functional hyperemia; neurovascular coupling; capillaries

## Introduction

Alzheimer's disease (AD) is currently the sixth-leading cause of death in the USA, with a death toll that continues to steeply increase. At present, ~56 million Americans suffer from AD or other forms of dementia, numbers that are expected to almost double by the year 2050.<sup>1</sup> The healthcare costs for the management of AD are substantial and impose a significant burden on society.<sup>2</sup> Accumulation of neurotoxic metabolites, such as amyloid  $\beta$  peptides and tau protein, neuronal loss, and pathological alterations in the brain vasculature are hallmarks of AD.<sup>3-11</sup> Notably, dynamic regulation of cerebral blood flow (CBF) in response to neuronal activity (functional hyperemia) is reduced during AD.<sup>6,9,12</sup> These CBF impairments are in a stark contrast to normal physiological circumstances in which the blood supply is efficiently coupled to neuronal activity, a process that is essential not only to meet real-time energy demands, but also to remove neuronal metabolic waste.<sup>13</sup>

Our previous work has established that brain capillaries, which lie in close proximity to all neurons, sense mediators released during neural activity. In particular, capillary endothelial cells (cECs) express inward-rectifier Kir2.1 channels that are activated by neuronally derived extracellular K<sup>+</sup>. Sensing of K<sup>+</sup> by capillaries triggers retrograde capillary-to-arteriole hyperpolarizing signals that dilate upstream penetrating arterioles and increase CBF.<sup>14</sup> We have further showed that cEC Kir2.1 activity and its role in CBF regulation are dynamically regulated by the phosphoinositide, phosphatidylinositol 4,5-bisphosphate (PIP<sub>2</sub>), consistent with earlier reports.<sup>15-20</sup> Interestingly, major disruptions in phosphoinositide levels have been reported in the brains of AD patients.<sup>21-24</sup> Furthermore, amyloid  $\beta$  reduces PIP<sub>2</sub> levels in cortical neurons,<sup>25,26</sup> and these metabolic perturbations presumably contribute to altered CBF and cognitive decline. However, whether AD affects the capillary endothelium

and more specifically cEC Kir2.1 channel function and electrical capillary-to-arteriole signaling, is unknown.

Here, we demonstrate that functional hyperemic responses are impaired in the somatosensory cortex of 5xFAD mice, a model of familial AD. We further show that this impairment is largely attributable to crippled capillary K<sup>+</sup> sensing due to reduced cEC Kir2.1 channel activity. Intriguingly, exogenous PIP<sub>2</sub> supplementation restored cEC Kir2.1 currents in isolated cECs and rescued deficits in K<sup>+</sup>-induced CBF and whisker stimulation (WS)-induced functional hyperemic responses *in vivo*. Collectively, our findings establish that diminished capillary Kir2.1 channel activity underlies the impaired CBF in 5xFAD mice. They further illustrate that restoration of electrical capillary signaling by exogenous supplementation of PIP<sub>2</sub> or a precursor is a potential novel therapeutic approach for the treatment of cerebral blood deficits in AD.

## Results

### Amyloid $\beta$ Accumulation in the 5xFAD Mouse Brain

In this study, we used 12-month-old 5xFAD model mice, which express human amyloid precursor protein containing four familial mutations found in AD patients and a mutant version of the human presenilin 1 gene.<sup>4</sup> To visualize amyloid  $\beta$  plaques in 5xFAD brains, we first injected mice with TRITC-dextran to visualize vascular networks and then created topological vascular maps up to 300  $\mu$ m deep in Layers I-III of the somatosensory cortex. We then stained  $\beta$ -amyloid peptide with the fluorescent marker, methoxy-X04. Topological maps showed a marked accumulation of amyloid  $\beta$  plaques dispersed throughout the cortex and around blood vessels in ~12-month-old 5xFAD mice, but not in age-matched controls (Figure 1A and B), consistent with disease progression.

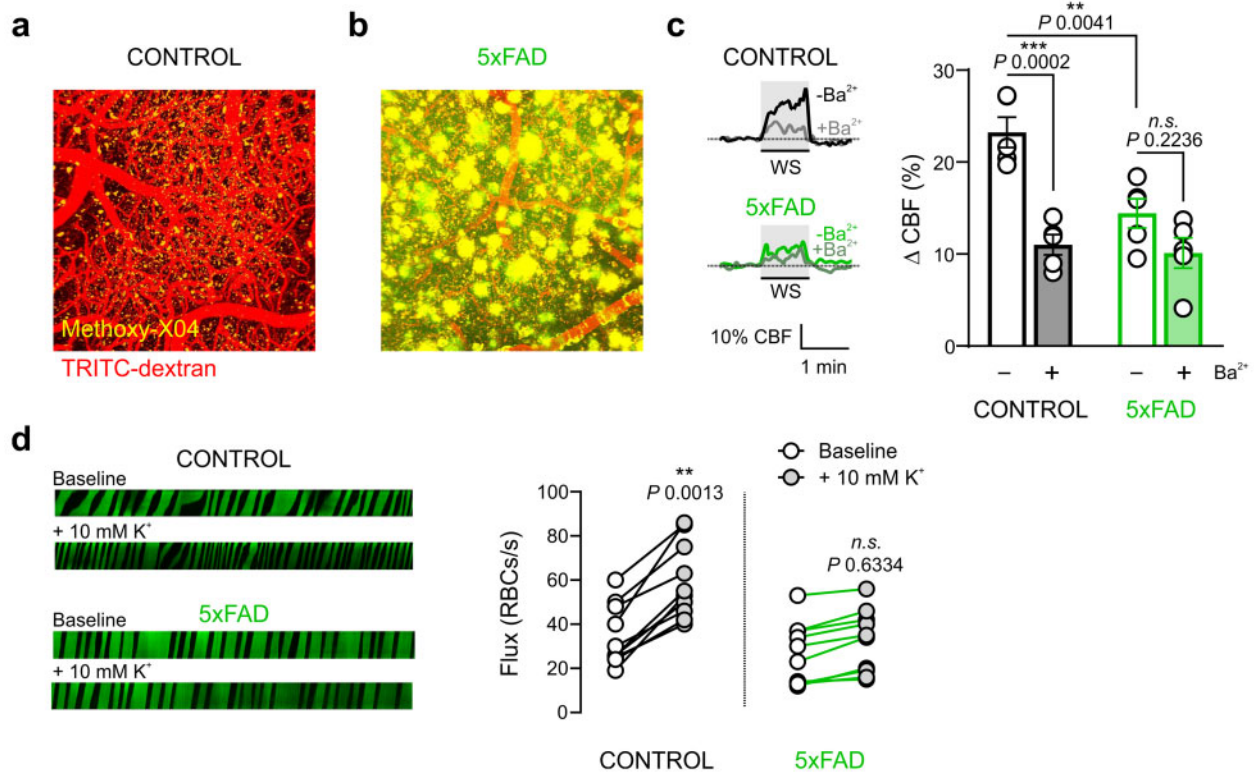


**Figure 1.** Functional Hyperemia is Impaired in 5xFAD Mice *In vivo*. Representative 3D *in vivo* images showing the vascular network (red) and  $\beta$ -amyloid plaques (yellow) accumulated in the cortex of (a) control and (b) 5xFAD mice. Block width =  $425 \times 425 \mu\text{m}$ ; block depth =  $300 \mu\text{m}$  ( $n = 3$  mice each). (c) Representative traces (left) and summary data (right) showing WS-induced changes in CBF in control and 5xFAD mice ( $n = 5$  mice each;  $**P < 0.01$ ,  $***P < 0.001$ , two-way ANOVA with Tukey's test as post hoc analysis). (d) Representative line scans (1 s each) and summary data showing RBC flux responses to 10 mM  $\text{K}^+$  in control (baseline,  $35 \pm 4$  cells/s; 10 mM  $\text{K}^+$ ,  $60 \pm 5$  cells/s;  $n = 10$  paired experiments, five mice) and 5xFAD mice (baseline,  $27 \pm 4$  cells/s; 10 mM  $\text{K}^+$ ,  $32 \pm 4$  cells/s;  $n = 10$  paired experiments, five mice).  $**P < 0.01$  (paired Student's *t*-test).

### WS-Induced Functional Hyperemic Responses and $\text{K}^+$ -Induced CBF Increases are Reduced During AD

We next used laser-Doppler flowmetry to assess functional hyperemic responses in anesthetized 5xFAD mice fitted with a cranial window. To this end, we first assessed changes in CBF induced in the somatosensory cortex of the contralateral hemisphere by repeated 60 s deflection of mouse vibrissae. WS evoked a profound increase in CBF in control mice ( $23.3 \pm 1.7\%$ ), as expected; however, the hyperemic response was markedly attenuated in 5xFAD mice ( $11.0 \pm 1.1\%$  increase). To assess the contribution of Kir2.1 channels to functional hyperemia, we measured CBF increases in the absence and presence of the Kir2 blocker,  $\text{Ba}^{2+}$  ( $100 \mu\text{M}$ ), applied to the cranial window. The  $\text{Ba}^{2+}$ -sensitive component of CBF was  $\sim 52\%$  in control mice. However, the effect of  $\text{Ba}^{2+}$  was not statistically significant in 5xFAD mice, suggesting impaired vascular Kir2.1 channel function (Figure 1C). We next directly tested capillary  $\text{K}^+$  sensing by focally stimulating post-arteriolar capillaries (third to fourth order) with 10 mM  $\text{K}^+$  while monitoring red blood cell (RBC) flux. Line scans of test capillaries showed that 10 mM  $\text{K}^+$  did not trigger an increase in RBC flux in 5xFAD mice; in contrast, RBC flux robustly increased in capillaries of age-matched controls ( $80.9\% \pm 14.1\%$ ) as we have previously reported<sup>14</sup> (Figure 1D).

### Kir2.1 Channel Activity is Suppressed in 5xFAD Capillaries

*In vivo* experiments suggested that capillary Kir2.1 activity—the cornerstone of  $\text{K}^+$ -induced capillary-to-arteriole signaling—is

crippled in 5xFAD mice. In subsequent experiments, we directly measured Kir2.1 channel currents in isolated cECs bathed in a 60-mM  $\text{K}^+$  solution in response to voltage ramps (from  $-140$  to  $+40$  mV) using the conventional whole-cell configuration of the patch-clamp technique and a pipette containing an intracellular solution lacking ATP. To minimize the impact of cytosolic dialysis on channel activity, currents were measured within  $\sim 3$ – $5$  min after gaining electrical access. These analyses showed that Kir2.1 current density was reduced by  $\sim 40\%$  in cECs from 5xFAD mice ( $-7.3$  pA/pF at  $-140$  mV) compared with controls ( $-12.2$  pA/pF; Figure 2A).

### PIP<sub>2</sub> Restores Kir2.1 Currents in 5xFAD cECs and Rescues $\text{K}^+$ -Induced CBF Increases and Functional Hyperemic Responses to WS in 5xFAD Mice

PIP<sub>2</sub> binding to the Kir2.1 channel is absolutely required for normal channel function,<sup>16–20</sup> and capillary Kir2.1 activity can be silenced by PIP<sub>2</sub> depletion.<sup>15</sup> Accordingly, we next tested whether PIP<sub>2</sub> supplementation was capable of restoring Kir2.1 currents in 5xFAD cECs. Strikingly, bath application of the water-soluble PIP<sub>2</sub> analog, diC16-PIP<sub>2</sub> ( $10 \mu\text{M}$ ), for  $\sim 20$  min followed by current recording showed an increase in Kir2.1 current density in 5xFAD cECs by  $\sim 90\%$  ( $-\text{PIP}_2$ :  $-7.5$  pA/pF;  $+\text{PIP}_2$ :  $-14$  pA/pF), without affecting cEC Kir2.1 current density in control cECs ( $-\text{PIP}_2$ :  $-12$  pA/pF;  $+\text{PIP}_2$ :  $-9.4$  pA/pF; Figure 2B–D).

To determine whether the corrective actions of PIP<sub>2</sub> on Kir2.1 currents in 5xFAD cECs translated to restoration of hyperemic responses, we tested whether systemic administration of PIP<sub>2</sub> rescued the impaired RBC flux response to capillary stimulation

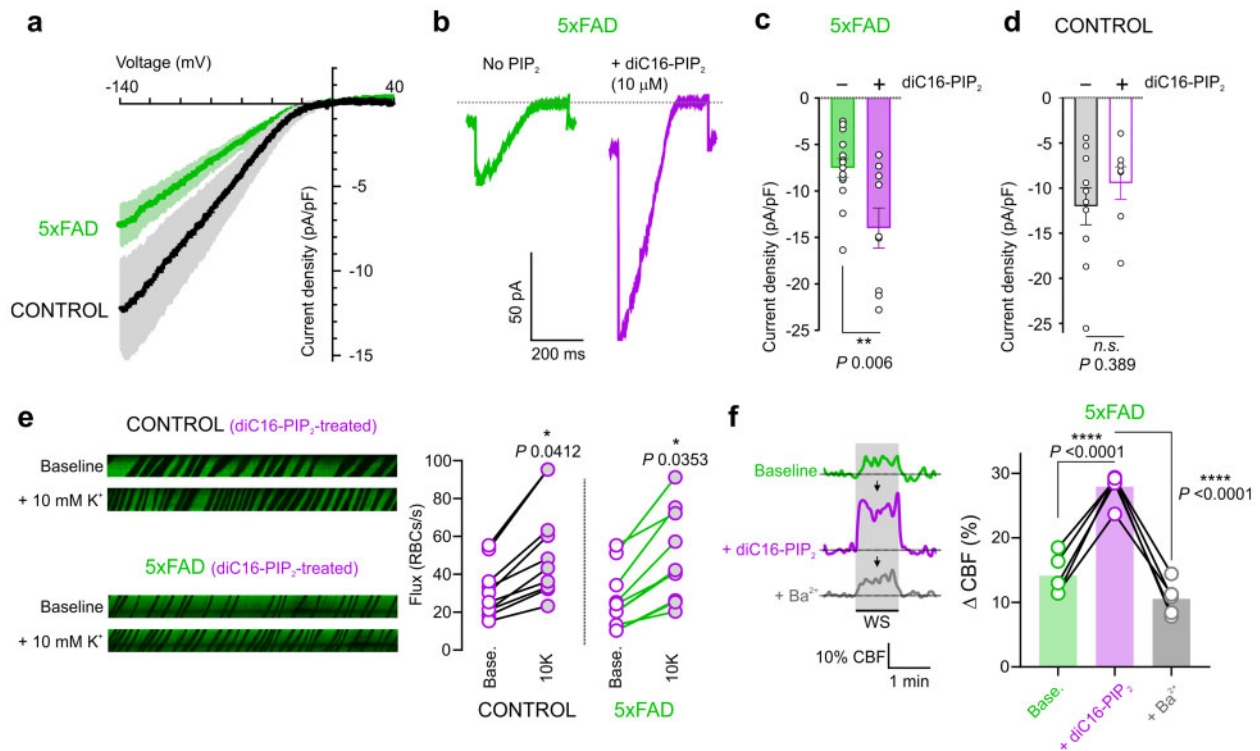


**Figure 2.** PIP<sub>2</sub> Restores Capillary Kir2.1 Channel Function and K<sup>+</sup> Sensing in 5xFAD Capillaries. (a) Averaged traces of Kir2.1 current in brain cECs from control (black; n = 10 cECs from four mice) and 5xFAD (green; n = 14 cECs from four mice) mice, recorded in the conventional whole-cell configuration using voltage ramps from -140 to +40 mV. Light colors indicate SEM. (b) Representative traces of Kir2.1 current in two 5xFAD cECs in the absence (green) or presence (purple) of diC16-PIP<sub>2</sub> in the bath solution, recorded using the same protocol as in Panel a. (c and d) Scatter-plot averages of inward current densities at -140 mV in 5xFAD (c) and control (d) cECs in the absence and presence of diC16-PIP<sub>2</sub> in the bath solution. (n = 7–14 cECs/group, n = 6 mice for both control and 5xFAD groups; \*\*P < 0.01; n.s., not significant; unpaired Student's t-test). For PIP<sub>2</sub> experiments, cECs were incubated with a bath solution supplemented with 10 μM diC16-PIP<sub>2</sub> for ~20 min prior to recordings. (e) Representative line scans and summary data showing RBC flux responses to 10 mM K<sup>+</sup> in control (baseline, 31 ± 4 cells/s; 10 mM K<sup>+</sup>, 53 ± 8 cells/s; n = 10 paired experiments, five mice) and 5xFAD mice (baseline: 26 ± 5 cells/s; 10 mM K<sup>+</sup>, 49 ± 7 cells/s; n = 10 paired experiments, five mice) 20 min after the systemic injection of diC16-PIP<sub>2</sub>. \*P < 0.05 (paired Student's t-test). (f) Representative traces (left) and summary data (right) showing WS-induced changes in CBF in 5xFAD mice before (baseline) and after the consecutive administration of diC16-PIP<sub>2</sub> (intravascular injection) and Ba<sup>2+</sup> (cranial window application) (n = 5 mice; \*\*\*\*P < 0.0001; one-way repeated measures ANOVA with Tukey's test for post hoc analysis).

with K<sup>+</sup>. To this end, we intravenously injected diC16-PIP<sub>2</sub> (0.5 mg/kg) and ~20 min post-injection we measured capillary RBC flux before and after focal application of 10 mM K<sup>+</sup> onto a capillary. Notably, hyperemic responses to 10 mM K<sup>+</sup> in 5xFAD mice were rescued by diC16-PIP<sub>2</sub> treatment (Figure 2E), which restored responses to levels comparable to those in controls (Figure 1D). PIP<sub>2</sub> treatment had no effect on K<sup>+</sup>-induced increases in RBC flux in control mice (Figure 2E). Finally, we assessed functional hyperemic responses to a physiological stimulus by measuring changes in CBF induced by WS in the presence of diC16-PIP<sub>2</sub>. In 5xFAD mice, systemic injection of diC16-PIP<sub>2</sub> (0.5 mg/kg) significantly increased the CBF response to WS ~20 min post-injection (Figure 2F), by enhancing the Ba<sup>2+</sup>-sensitive component.

## Discussion

Accumulating evidence has established a crucial role for the endothelium,<sup>27,28</sup> and particularly the capillary endothelium,<sup>14</sup> in mediating neurovascular coupling and thereby regulating CBF. Endothelial dysfunction has also been implicated in cerebral vascular diseases.<sup>29–31</sup> However, despite a general appreciation of the role of vascular dysfunction in stroke and atherosclerosis, the involvement of endothelial dysfunction in the

pathophysiology of AD is not fully understood.<sup>32–34</sup> AD patients display reductions in CBF in various regions of brain, including the cortex and the hippocampus in conjunction with cognitive dementia.<sup>9,35,36</sup> Whether the contribution of capillary-to-arteriole signaling—and therefore CBF control—is affected during AD has not been explored. In this study, we provide evidence for a novel pathomechanism underlying a capillary Kir2.1 channelopathy that leads to impaired functional hyperemia during AD. Importantly, we further show that systemic administration of the co-factor, PIP<sub>2</sub>, restores Kir2.1 channel function and the capillary-to-arteriole signaling that triggers hyperemic responses.

The brain capillary Kir2.1 channel is an ideal sensor of neural activity by virtue of its biophysical properties.<sup>37,38</sup> Modest elevations of extracellular [K<sup>+</sup>]<sub>o</sub> activate cEC Kir2.1 channels, initiating a retrograde hyperpolarizing signal that dilates upstream arterioles and increases blood flow at the initiation site.<sup>14</sup> Moreover, the phosphoinositide PIP<sub>2</sub> is indispensable for normal Kir2.1 channel function;<sup>39,40</sup> in fact, PIP<sub>2</sub> depletion deactivates cEC Kir2.1 channels and eliminates capillary-to-arteriole signaling.<sup>15</sup> The present study shows that capillary Kir2.1 function is crippled in a mouse model of AD. These findings further highlight the importance of vascular Kir2.1 channels in a variety of pathologies, including ischemia,<sup>41</sup> stress,<sup>42</sup> hypertension,<sup>43</sup> and AD.<sup>5</sup>

Amyloid  $\beta$  has been shown to induce endothelial dysfunction and impair endothelium-dependent vasodilation.<sup>32,33</sup> Amyloid  $\beta$  peptides additionally interact with anionic phospholipids, such as PIP<sub>2</sub>,<sup>44</sup> and increase phospholipase-mediated PIP<sub>2</sub> hydrolysis.<sup>45</sup> Intriguingly, several studies have reported a reduction in membrane phospholipids, including PIP<sub>2</sub>, in the brains of AD patients.<sup>21–23,46</sup> This reduced availability of PIP<sub>2</sub> could reflect disrupted PIP<sub>2</sub> synthesis or metabolism.<sup>47</sup> PIP<sub>2</sub> synthesis is mediated by lipid kinases, which require relatively high concentrations of ATP (hundreds-of-micromolar range) compared with protein kinases (low-micromolar range); thus, the phosphorylation potential of their substrates is greatly influenced by ADP:ATP ratio. Notably, AD patients and mouse models also show reduced levels of ATP in their brains,<sup>48,49</sup> although whether this underlies reduced PIP<sub>2</sub> availability remains unknown. Nevertheless, our data provide strong evidence that exogenous administration of PIP<sub>2</sub> reverses cEC Kir2.1 channel dysfunction and restores the K<sup>+</sup>-sensing function of brain capillaries in 5xFAD mice. Exogenous PIP<sub>2</sub> can presumably be transported to the inner leaflet of the plasma membrane by scramblases and/or flippases, further investigations addressing this possibility are warranted. Therefore, the restoration of cEC Kir2.1 channel function by PIP<sub>2</sub> could improve functional hyperemia and CBF responses in the setting of AD. These observations have enormous translational potential and suggest novel therapeutic strategies for the treatment not only of AD, but also of other cerebrovascular and neurodegenerative diseases in which CBF is disrupted. Developing these therapeutic manipulations is crucial to improving the quality of life of the growing elderly population experiencing cognitive decline and dementia.<sup>1</sup>

In conclusion, this study reports a novel Kir2.1 channelopathy in brain capillaries that contributes to impaired CBF control in a mouse model of AD. Importantly, administration of the cofactor PIP<sub>2</sub> corrected capillary Kir2.1 channel dysfunction and restored hyperemic responses to normal levels. Therefore, our data establish the foundation for a therapeutic approach for improving CBF in AD, one that may also be relevant in ischemic stroke and other diseases where CBF is crippled.

## Material and Methods

### Animal Husbandry

All experimental protocols used in this study are in accord with institutional guidelines approved by the Institutional Animal Care and Use Committee of the University of Vermont. All procedures were conducted and reported in accordance with ARRIVE guidelines. Male and female 5xFAD mice (JAX: 34840, Tg<sup>+</sup>) and age-matched littermate controls were used for the study. Mice were used at 12–13 months of age because prior work showed significant loss of neuronal activity at about 12 months.<sup>50,51</sup> Mice were housed in groups of four on a 12-h light/dark cycle, with ad libitum access to food and water. For cell isolation, animals were euthanized by intraperitoneal injection of sodium pentobarbital (100 mg/kg) followed by rapid decapitation.

### Cortical CBF Measurements In vivo

WS-induced functional hyperemic responses were measured using laser-Doppler flowmetry as previously described,<sup>14,52</sup> with some modifications. Briefly, mice were initially anesthetized with isoflurane (5% induction, 2% maintenance) and their

femoral artery was cannulated for monitoring blood pressure. An acute cranial window (~2-mm diameter) was created over the somatosensory cortex and superfused with aerated warm (~37°C) artificial cerebrospinal fluid (aCSF; 124 mM NaCl, 3 mM KCl, 2 mM CaCl<sub>2</sub>, 2 mM MgCl<sub>2</sub>, 1.25 mM NaH<sub>2</sub>PO<sub>4</sub>, 26 mM NaHCO<sub>3</sub>, and 4 mM glucose). Isoflurane anesthesia was replaced with the combination of  $\alpha$ -chloralose (50 mg/kg; i.p.) and urethane (750 mg/kg; i.p.) at the conclusion of the surgery. Cortical CBF was measured with a laser-Doppler probe (PeriMed), and functional hyperemic responses were induced by stroking the contralateral vibrissae for 1 min (~3 Hz). Changes in CBF were expressed relative to baseline values as a percentage. Blood pressure was monitored throughout the experiment (mean arterial pressure; age-matched controls: 114  $\pm$  2 mmHg; 5xFAD: 111  $\pm$  4 mmHg), and body temperature was maintained at 37°C using a servo-controlled heating pad with a rectal temperature sensor probe. All data were recorded and analyzed using LabChart software (AD Instruments).

### In vivo Imaging of Cerebral Hemodynamics

*In vivo* imaging was performed as previously described.<sup>14</sup> Briefly, mice were anesthetized with isoflurane (5% induction, 2% maintenance), and a stainless-steel head plate was attached to the exposed skull with a mixture of dental cement and glue. An acute small (~2-mm diameter) circular cranial window was created over the somatosensory cortex (~–1.5 mm anterior-posterior, 3.0 mm medial-lateral relative to bregma). Approximately 150  $\mu$ L of FITC-dextran (3 mg/mL; molecular weight, 150 kDa) in saline was injected intravenously into the retro-orbital sinus to allow visualization of the cerebral vasculature and contrast imaging of RBCs. Upon conclusion of surgery, isoflurane anesthesia was replaced with  $\alpha$ -chloralose (50 mg/kg; i.p.) and urethane (750 mg/kg; i.p.). Body temperature was maintained at 37°C throughout the experiment using an electric heating pad. For staining of amyloid  $\beta$  plaques, 150  $\mu$ L of a solution containing methoxy-X04 (1  $\mu$ M) and TRITC-dextran (3 mg/mL; molecular weight, 150 kDa) in saline was injected intravenously. For K<sup>+</sup>-evoked hyperemia experiments, a pipette was maneuvered into the cortex and positioned adjacent to a capillary downstream of an arteriole (first to third branch order), after which aCSF containing 10 mM K<sup>+</sup> was ejected directly onto the capillary (300 ms, 6  $\pm$  1 psi), producing a small plume of solution. Spatial coverage of the ejected solution was monitored by including TRITC-dextran (150 kDa; 0.2 mg/mL) in the pipette. For PIP<sub>2</sub>-supplementation experiments, diC16-PIP<sub>2</sub> (0.5 mg/kg) was systemically administered via intravenous injections and capillary stimulation was performed 20 min after injections. Systemic injections of diC16-PIP<sub>2</sub> did not alter mean arterial pressure in 5xFAD or control mice. RBC flux data were collected by line scanning the capillary of interest at 5 kHz. Images were acquired using a Zeiss LSM-7 multiphoton microscope (Zeiss, USA) equipped with a 20 $\times$  Plan Apochromat 1.0 N.A. DIC VIS-IR water-immersion objective and coupled to a Coherent Chameleon Vision II Titanium-Sapphire pulsed infrared laser (Coherent, USA). FITC, TRITC, and methoxy-X04 were excited at 820 nm, and emitted fluorescence was separated through emission filters of 420–500 nm (methoxy-X04), 500–550 nm (FITC), and 570–610 nm (TRITC) bandpass filters.

### cEC Isolation

Single cECs were obtained from mouse brains by mechanical disruption of a volume of ~10–15 mm<sup>3</sup> of somatosensory

cortical tissue using a Dounce homogenizer, as previously described.<sup>14</sup> Briefly, slices were homogenized in ice-cold isolation solution (124 mM NaCl, 3 mM KCl, 2 mM CaCl<sub>2</sub>, 2 mM MgCl<sub>2</sub>, 1.25 mM NaH<sub>2</sub>PO<sub>4</sub>, 26 mM NaHCO<sub>3</sub>, and 4 mM glucose) and debris was removed by passing the homogenate through a 62- $\mu$ m nylon mesh. Retained capillary fragments were washed into dissociation solution composed of 55 mM NaCl, 80 mM Na-glutamate, 5.6 mM KCl, 2 mM MgCl<sub>2</sub>, 4 mM glucose, and 10 mM HEPES (pH 7.3) containing neutral protease (0.5 mg/mL), elastase (0.5 mg/mL; Worthington, USA) and 100  $\mu$ M CaCl<sub>2</sub>, and then incubated for 23 min at 37°C. Thereafter, 0.5 mg/mL collagenase Type I (Worthington, USA) was added for an additional 2 min incubation at 37°C. Enzymes were removed by filtering and washing the suspension, and single cells and small capillary fragments were dispersed by triturating 4–7 times with a fire-polished glass Pasteur pipette. Cells were used within ~6 h of dispersion.

### Electrophysiology

Whole-cell currents were recorded as previously described<sup>15</sup> using a patch-clamp amplifier (Axopatch 200B; Molecular Devices, San Jose, CA), filtered at 1 kHz, digitized at 5 kHz, and stored on a computer for offline analysis with Clampfit version 10.3 software. Whole-cell capacitance was measured using the cancellation circuitry in the voltage-clamp amplifier. Electrophysiological analyses were performed in the conventional whole-cell configuration. Recording pipettes were fabricated by pulling borosilicate glass (1.5 mm outer diameter, 1.17 mm inner diameter; Sutter Instruments, USA) using a Narishige puller. Pipettes were fire-polished to a tip resistance of ~4–5 M $\Omega$ . The bath solution consisted of 80 mM NaCl, 60 mM KCl, 1 mM MgCl<sub>2</sub>, 10 mM HEPES, 4 mM glucose, and 2 mM CaCl<sub>2</sub> (pH 7.4). Pipettes were backfilled with a solution consisting of 10 mM NaOH, 11.4 mM KOH, 128.6 mM KCl, 1.1 mM MgCl<sub>2</sub>, 2.2 mM CaCl<sub>2</sub>, 5 mM EGTA, and 10 mM HEPES (pH 7.2). Recordings were made within ~3–5 min after gaining electrical access to the interior of the cell. In a subset of experiments, the bath solution was supplemented with diC16-PIP<sub>2</sub> analog, as indicated in the text.

### Statistical Analysis

Patch-clamp data were analyzed using Clampfit version 10.7 software. RBC flux was analyzed offline using custom software (SparkAn, Adrian Bonev, University of Vermont, USA). Flux data were binned at 1-s intervals. Mean baseline velocity and flux data for summary figures were obtained by averaging the baseline (~6 s) for each measurement before pressure ejection of 10 mM K<sup>+</sup>. The peak response was defined as the peak 1-s flux bin after delivery of K<sup>+</sup> within the remaining scanning period (~54 s). The depth of capillaries below the surface was estimated from z-stack series acquired before pipette placement. Results are presented as means  $\pm$  standard error of the mean (SEM), and *n* refers to the number of animals used, unless otherwise stated. Statistical significance was determined with GraphPad Prism version 8 software using either two-tailed Student's *t*-test or Analysis of Variance (ANOVA; one or two way) with Tukey's test as *post hoc* analysis, as specified in figure legends. *P*-value <0.05 was considered statistically significant.

### Acknowledgments

The authors thank Dr. Grant Hennig for technical assistance.

### Funding

This work was supported by Postdoctoral Fellowships (20POST35210155 to A.M.; 17POST33650030 to O.F.H.), and a Career Development Award (20CDA35310097 to O.F.H.) from the American Heart Association (AHA), an Early Career Research Award (to A.M.) and Career Development Awards (to A.M. and O.F.H.) from the Cardiovascular Research Institute at the University of Vermont. Additional support was provided by the Totman Medical Research Trust (to M.T.N.), the Fondation Leducq Transatlantic Network of Excellence on the Pathogenesis of Small Vessel Disease of the Brain (to M.T.N.), European Union's Horizon 2020 Research and Innovation Program (Grant Agreement 666881, SVDs@target, to M.T.N.), a grant from the Henry M. Jackson Foundation for the Advancement of Military Medicine (HU0001-18-2-0016), and grants from the National Institutes of Health (K01-HL-138215 to A.L.G., P01-HL-095488, R01-HL-121706, R37-DK-053832, 7UM-HL-1207704, and R01-HL-131181 to M.T.N.). Research was also supported by grants from the National Institute of Neurological Disorders and Stroke (NINDS) and National Institute of Aging (NIA; R01-NS-110656 to M.T.N.), the National Institute of General Medical Sciences (NIGMS; P20-GM-135007; PIs: Mary Cushman and Mark Nelson, Vermont Center for Cardiovascular and Brain Health [to O.F.H.]), and by the National Heart, Lung, and Blood Institute (NHLBI) of the NIH under Award number R35-HL-140027 (to M.T.N.).

### Authors' Contributions

A.M. and O.F.H. designed experiments, acquired and analyzed data, and wrote the manuscript. A.L.G. and D.H.-E. edited the manuscript. M.T.N. directed the research and wrote the manuscript. All authors reviewed the manuscript and approved its submission.

### Conflict of Interest Statement

O.F.H. and M.T.N. are inventors of patent number 62/823,378 "Methods to promote cerebral blood flow in the brain" which was submitted on March 25, 2019. M.N. holds the position of Executive Editor for *Function* and is blinded from reviewing or making decisions for the manuscript.

### References

- 2020 Alzheimer's disease facts and figures. *Alzheimers Dement* 2020;16:391–460.doi: 10.1002/alz.12068.
- Hurd MD, Martorell P, Langa KM. Monetary costs of dementia in the United States. *N Engl J Med* 2013;369(5):489–490.
- Park L, Hochrainer K, Hattori Y, et al. Tau induces PSD95-neuronal NOS uncoupling and neurovascular dysfunction independent of neurodegeneration. *Nat Neurosci* 2020;23(9):1079–1089.
- Oakley H, Cole SL, Logan S, et al. Intraneuronal  $\beta$ -amyloid aggregates, neurodegeneration, and neuron loss in transgenic mice with five familial Alzheimer's disease mutations: potential factors in amyloid plaque formation. *J Neurosci* 2006; 26(40):10129–10140.
- Hakim MA, Behringer EJ. Development of Alzheimer's disease progressively alters sex-dependent K<sub>Ca</sub> and sex-independent

- K<sub>IR</sub> channel function in cerebrovascular endothelium. *J Alzheimers Dis* 2020;76(4):1423–1442.
6. Park L, Wang G, Moore J, et al. The key role of transient receptor potential melastatin-2 channels in amyloid- $\beta$ -induced neurovascular dysfunction. *Nat Commun* 2014;5:5318. doi: 10.1038/ncomms6318.
  7. Roher AE, Debbins JP, Malek-Ahmadi M, et al. Cerebral blood flow in Alzheimer's disease. *Vasc Health Risk Manag* 2012;8:599–611. doi: 10.2147/VHRM.S34874.
  8. Zheng W, Cui B, Han Y, et al. Disrupted regional cerebral blood flow, functional activity and connectivity in Alzheimer's disease: a combined ASL perfusion and resting state fMRI study. *Front Neurosci* 2019;13:738. doi: 10.3389/fnins.2019.00738.
  9. Niwa K, Younkin L, Ebeling C, et al. A $\beta$ 1-40-related reduction in functional hyperemia in mouse neocortex during somatosensory activation. *Proc Natl Acad Sci USA* 2000;97(17):9735–9740.
  10. Tarantini S, Fulop GA, Kiss T, et al. Demonstration of impaired neurovascular coupling responses in TG2576 mouse model of Alzheimer's disease using functional laser speckle contrast imaging. *Geroscience* 2017;39(4):465–473.
  11. Iadecola C, Gottesman RF. Cerebrovascular alterations in Alzheimer disease. *Circ Res* 2018;123(4):406–408.
  12. Girouard H, Iadecola C. Neurovascular coupling in the normal brain and in hypertension, stroke, and Alzheimer disease. *J Appl Physiol* (1985) 2006;100(1):328–335.
  13. Iadecola C. The neurovascular unit coming of age: a journey through neurovascular coupling in health and disease. *Neuron* 2017;96(1):17–42.
  14. Longden TA, Dabertrand F, Koide M, et al. Capillary K<sup>+</sup>-sensing initiates retrograde hyperpolarization to increase local cerebral blood flow. *Nat Neurosci* 2017;20(5):717–726.
  15. Harraz OF, Longden TA, Dabertrand F, Hill-Eubanks D, Nelson MT. Endothelial GqPCR activity controls capillary electrical signaling and brain blood flow through PIP<sub>2</sub> depletion. *Proc Natl Acad Sci USA* 2018;115(15):E3569–E3577.
  16. Huang CL, Feng S, Hilgemann DW. Direct activation of inward rectifier potassium channels by PIP<sub>2</sub> and its stabilization by G $\beta$ s. *Nature* 1998;391(6669):803–806.
  17. Hansen SB, Tao X, MacKinnon R. Structural basis of PIP<sub>2</sub> activation of the classical inward rectifier K<sup>+</sup> channel Kir2.2. *Nature* 2011;477(7365):495–498.
  18. D'Avanzo N, Cheng WW, Doyle DA, Nichols CG. Direct and specific activation of human inward rectifier K<sup>+</sup> channels by membrane phosphatidylinositol 4,5-bisphosphate. *J Biol Chem* 2010;285(48):37129–37132.
  19. D'Avanzo N, Lee SJ, Cheng WW, Nichols CG. Energetics and location of phosphoinositide binding in human Kir2.1 channels. *J Biol Chem* 2013;288(23):16726–16737.
  20. Du X, Zhang H, Lopes C, Mirshahi T, Rohacs T, Logothetis DE. Characteristic interactions with phosphatidylinositol 4,5-bisphosphate determine regulation of kir channels by diverse modulators. *J Biol Chem* 2004;279(36):37271–37281.
  21. Jope RS, Song L, Li X, Powers R. Impaired phosphoinositide hydrolysis in Alzheimer's disease brain. *Neurobiol Aging* 1994;15(2):221–226.
  22. Stokes CE, Hawthorne JN. Reduced phosphoinositide concentrations in anterior temporal cortex of Alzheimer-diseased brains. *J Neurochem* 1987;48(4):1018–1021.
  23. Wallace MA. Effects of Alzheimer's disease-related beta amyloid protein fragments on enzymes metabolizing phosphoinositides in brain. *Biochim Biophys Acta* 1994;1227(3):183–187.
  24. Landman N, Jeong SY, Shin SY, et al. Presenilin mutations linked to familial Alzheimer's disease cause an imbalance in phosphatidylinositol 4,5-bisphosphate metabolism. *Proc Natl Acad Sci USA* 2006;103(51):19524–19529.
  25. Berman DE, Dall'Armi C, Voronov SV, et al. Oligomeric amyloid- $\beta$  peptide disrupts phosphatidylinositol-4,5-bisphosphate metabolism. *Nat Neurosci* 2008;11(5):547–554.
  26. Zhu L, Zhong M, Elder GA, et al. Phospholipid dysregulation contributes to ApoE4-associated cognitive deficits in Alzheimer's disease pathogenesis. *Proc Natl Acad Sci USA* 2015;112(38):11965–11970.
  27. Chen BR, Kozberg MG, Bouchard MB, Shaik MA, Hillman EM. A critical role for the vascular endothelium in functional neurovascular coupling in the brain. *J Am Heart Assoc* 2014;3(3):e000787.
  28. Chow BW, Nunez V, Kaplan L, et al. Caveolae in CNS arterioles mediate neurovascular coupling. *Nature* 2020;579(7797):106–110.
  29. Iadecola C, Duering M, Hachinski V, et al. Vascular cognitive impairment and dementia: JACC scientific expert panel. *J Am Coll Cardiol* 2019;73(25):3326–3344.
  30. Wardlaw JM, Smith C, Dichgans M. Small vessel disease: mechanisms and clinical implications. *Lancet Neurol* 2019;18(7):684–696.
  31. de Boer I, Stam AH, Buntinx L, et al. RVCL-S and CADASIL display distinct impaired vascular function. *Neurology* 2018;91(10):e956–e963.
  32. Price JM, Sutton ET, Hellermann A, Thomas T.  $\beta$ -Amyloid induces cerebrovascular endothelial dysfunction in the rat brain. *Neurol Res* 1997;19(5):534–538.
  33. Thomas T, McLendon C, Sutton ET, Thomas G. Cerebrovascular endothelial dysfunction mediated by  $\beta$ -amyloid. *Neuroreport* 1997;8(6):1387–1391.
  34. Takano T, Han X, Deane R, Zlokovic B, Nedergaard M. Two-photon imaging of astrocytic Ca<sup>2+</sup> signaling and the microvasculature in experimental mice models of Alzheimer's disease. *Ann N Y Acad Sci* 2007;1097:40–50.
  35. Niwa K, Carlson GA, Iadecola C. Exogenous A $\beta$ 1-40 reproduces cerebrovascular alterations resulting from amyloid precursor protein overexpression in mice. *J Cereb Blood Flow Metab* 2000;20(12):1659–1668.
  36. de Jong DLK, de Heus RAA, Rijpmma A, et al. Effects of nilvadipine on cerebral blood flow in patients with Alzheimer disease. *Hypertension* 2019;74(2):413–420.
  37. Longden TA, Nelson MT. Vascular inward rectifier K<sup>+</sup> channels as external K<sup>+</sup> sensors in the control of cerebral blood flow. *Microcirculation* 2015;22(3):183–196.
  38. Hibino H, Inanobe A, Furutani K, Murakami S, Findlay I, Kurachi Y. Inwardly rectifying potassium channels: their structure, function, and physiological roles. *Physiol Rev* 2010;90(1):291–366.
  39. Sancho M, Fabris S, Hald BO, et al. Membrane lipid-K<sub>IR</sub>2.x channel interactions enable hemodynamic sensing in cerebral arteries. *Arterioscler Thromb Vasc Biol* 2019;39(6):1072–1087.
  40. Xie LH, John SA, Ribalet B, Weiss JN. Phosphatidylinositol-4,5-bisphosphate (PIP<sub>2</sub>) regulation of strong inward rectifier Kir2.1 channels: multilevel positive cooperativity. *J Physiol* 2008;586(7):1833–1848.
  41. Povlsen GK, Longden TA, Bonev AD, Hill-Eubanks DC, Nelson MT. Uncoupling of neurovascular communication after transient global cerebral ischemia is caused by impaired parenchymal smooth muscle Kir channel function. *J Cereb Blood Flow Metab* 2016;36(7):1195–1201.
  42. Longden TA, Dabertrand F, Hill-Eubanks DC, Hammack SE, Nelson MT. Stress-induced glucocorticoid signaling remodels neurovascular coupling through impairment of cerebrovascular inwardly rectifying K<sup>+</sup> channel function. *Proc Natl Acad Sci USA* 2014;111(20):7462–7467.

43. Gradel AKJ, Salomonsson M, Sorensen CM, Holstein-Rathlou NH, Jensen LJ. Long-term diet-induced hypertension in rats is associated with reduced expression and function of small artery SK<sub>Ca</sub>, IK<sub>Ca</sub>, and Kir2.1 channels. *Clin Sci (Lond)* 2018;132(4):461–474.
44. Chauhan A, Ray I, Chauhan VP. Interaction of amyloid beta-protein with anionic phospholipids: possible involvement of Lys28 and C-terminus aliphatic amino acids. *Neurochem Res* 2000;25(3):423–429.
45. Strosznajder JB, Zambrzycka A, Kacprzak MD, Strosznajder RP. Amyloid  $\beta$  peptide 25-35 modulates hydrolysis of phosphoinositides by membrane phospholipase(s) C of adult brain cortex. *J Mol Neurosci* 1999;12(2):101–109.
46. Klein J. Membrane breakdown in acute and chronic neurodegeneration: focus on choline-containing phospholipids. *J Neural Transm (Vienna)* 2000;107(8–9):1027–1063.
47. Harraz OF, Hill-Eubanks D, Nelson MT. PIP<sub>2</sub>: a critical regulator of vascular ion channels hiding in plain sight. *Proc Natl Acad Sci USA* 2020;117(34):20378–20389.
48. Zhang C, Rissman RA, Feng J. Characterization of ATP alterations in an Alzheimer's disease transgenic mouse model. *J Alzheimers Dis* 2015;44(2):375–378.
49. Beck SJ, Guo L, Phensy A, et al. Deregulation of mitochondrial F1FO-ATP synthase via OSCP in Alzheimer's disease. *Nat Commun* 2016;7:11483.
50. Eimer WA, Vassar R. Neuron loss in the 5XFAD mouse model of Alzheimer's disease correlates with intraneuronal A $\beta$ 42 accumulation and Caspase-3 activation. *Mol Neurodegener* 2013; 8:2. doi: 10.1186/1750-1326-8-2.
51. Jawhar S, Trawicka A, Jenneckens C, Bayer TA, Wirths O. Motor deficits, neuron loss, and reduced anxiety coinciding with axonal degeneration and intraneuronal Abeta aggregation in the 5XFAD mouse model of Alzheimer's disease. *Neurobiol Aging* 2012;33(1):196.e129–140.
52. Girouard H, Bonev AD, Hannah RM, Meredith A, Aldrich RW, Nelson MT. Astrocytic endfoot Ca<sup>2+</sup> and BK channels determine both arteriolar dilation and constriction. *Proc Natl Acad Sci USA* 2010;107(8):3811–3816.